






Geophysical Research Letters®

RESEARCH LETTER

10.1029/2024GL110583

A. Broquet and F. Rolser contributed equally to this work

Mercury's Crustal Porosity as Constrained by the Planet's Bombardment History

A. Broquet¹ , F. Rolser^{1,2} , A. C. Plesa¹ , D. Breuer¹ , and H. Hussmann¹ 

¹Institute for Planetary Research, German Aerospace Center, DLR, Berlin, Germany, ²Geophysical Institute, Karlsruhe Institute of Technology, KIT, Karlsruhe, Germany

Key Points:

- Mercury's crustal porosity estimated from the crater population, assuming porosity formed by large impacts and decreased with surface aging
- Crustal porosity in the cratered terrains ranges from 9% to 18% with an average and standard deviation of $13\% \pm 2\%$
- The low bulk density of Mercury's crust in the cratered terrain, $2,565 \pm 70 \text{ kg m}^{-3}$, is similar to that of the lunar highlands

Supporting Information:

Supporting Information may be found in the online version of this article.

Correspondence to:

A. Broquet,
adrien.broquet@dlr.de

Citation:

Broquet, A., Rolser, F., Plesa, A. C., Breuer, D., & Hussmann, H. (2024). Mercury's crustal porosity as constrained by the planet's bombardment history. *Geophysical Research Letters*, 51, e2024GL110583. <https://doi.org/10.1029/2024GL110583>

Received 31 MAY 2024

Accepted 23 OCT 2024

Author Contributions:

Conceptualization: A. Broquet, F. Rolser, A. C. Plesa, D. Breuer, H. Hussmann
Data curation: A. Broquet, F. Rolser
Formal analysis: A. Broquet, F. Rolser
Investigation: A. Broquet
Methodology: A. Broquet, F. Rolser, A. C. Plesa, D. Breuer, H. Hussmann
Project administration: A. Broquet
Resources: A. Broquet
Software: A. Broquet, F. Rolser
Supervision: A. Broquet, A. C. Plesa, D. Breuer, H. Hussmann
Validation: A. Broquet, F. Rolser

© 2024. The Author(s).

This is an open access article under the terms of the [Creative Commons Attribution-NonCommercial-NoDerivs License](#), which permits use and distribution in any medium, provided the original work is properly cited, the use is non-commercial and no modifications or adaptations are made.

Abstract Knowing the structure of the crust is critical to understanding a planet's geologic evolution. Crustal thickness inversions rely on bulk density estimates, which are primarily affected by porosity. Due to the absence of high-resolution gravity data, Mercury's crustal porosity has remained unknown. Here, we use a model that was calibrated to the Moon to relate Mercury's impact crater population and long-wavelength crustal porosity in the cratered terrains. Therein, porosity is created by large impacts and then decreased as the surface ages due to pore compaction by smaller impacts and overburden pressure. Our models fit independent gravity-derived porosity estimates in the northern regions, where data is well resolved. Porosity in the cratered terrains is found to be 9%–18% with an average and standard deviation of $13\% \pm 2\%$, indicating lunar-like crustal bulk densities of $2,565 \pm 70 \text{ kg m}^{-3}$ from which updated crustal thickness maps are constructed.

Plain Language Summary The crust of a planet is a thermal barrier, which controls how fast heat escapes to space. Depending on its thickness, the crust can strongly insulate the planet's interior preventing efficient cooling. Therefore, knowing the structure of the crust is critical to unraveling the geologic history of planetary bodies. Crustal thickness is typically inverted from gravity and topography data. One critical parameter for these inversions is the bulk density of the crust, which is primarily driven by porosity variations. While high-resolution gravity field mapping allowed constraining the bulk density and porosity of the lunar crust, crustal porosity on other planetary bodies has remained unknown. In this work, we use a model that was calibrated to the Moon to relate Mercury's impact crater population and long-wavelength crustal porosity in the cratered terrains. We show that crustal porosity in the cratered terrains ranges from 9% to 18% with an average and standard deviation of $13\% \pm 2\%$, indicating lunar-like low bulk densities of $2,565 \pm 70 \text{ kg m}^{-3}$.

1. Introduction

The crust of Mercury has been the stage for various geological processes, including volcanism (Head et al., 2011; Kiefer & Murray, 1987), the formation of giant impact basins (Fassett et al., 2012), but also global contraction and tectonic activity (Watters et al., 2004). Each of these processes has profoundly affected the structure, composition, and porosity of the crust. Both the thickness and porosity of Mercury's crust are critical to modeling the thermal, geologic, and tectonic evolution of the planet through time (Tosi et al., 2013; Watters et al., 2021). Classical inversions for crustal thickness rely on appropriate knowledge of the planetary gravity field and topography (e.g., Wiczorek et al., 2022) and, if available, additional constraints on the density and thickness of the crust from orbital analyses and seismic measurements (Knappmeyer-Endrun et al., 2021; Wiczorek et al., 2013). Given the lack of high-resolution gravity data for Mercury due to the high-altitude and elliptical orbit of the Mercury Surface, Space ENvironment, GEochemistry, and Ranging (MESSENGER) spacecraft (Smith et al., 2012), the thickness and in particular the porosity of the planet's crust have remained poorly known (Beuthe et al., 2020; Genova et al., 2023).

On the Moon, the high resolution gravity field derived from the Gravity Recovery And Interior Laboratory (GRAIL) mission allowed constraining both the thickness and bulk density of the crust (e.g., Broquet & Andrews-Hanna, 2024; Goossens et al., 2020; Wiczorek et al., 2013). In these models, variations in the crustal bulk density from composition and porosity dominantly affect the inverted crustal thickness. Interestingly, a study by Huang et al. (2022) found a remarkable inverse correlation between the long-wavelength ($\sim 1,000 \text{ km}$) GRAIL-derived crustal porosity in the lunar highlands and an independently mapped population of impact craters with diameter $>20 \text{ km}$. Coupled with a simple parameterized model under the assumption that crustal porosity variations are driven by impact brecciation and surface aging, the study was able to closely reproduce the GRAIL-derived lunar

Visualization: A. Broquet, F. Rolser

Writing – original draft: A. Broquet,
F. Rolser, A. C. Plesa, D. Breuer,
H. Hussmann

Writing – review & editing: A. Broquet,
F. Rolser, A. C. Plesa, D. Breuer,
H. Hussmann

highlands' crustal porosity. The topography of planetary bodies, which holds the cratering record, is generally better known than the gravity field. Therefore, the crater population derived from topography could act as a surrogate to provide information on the crustal porosity of planetary bodies with low-resolution gravity data.

Compared to the Moon with degree-1,200 gravity field models (Goossens et al., 2020), Mercury's gravity field is poorly known with resolution ranging from degree 10 (wavelength of $\sim 1,500$ km) in the southern hemisphere to 90 and up to 160 in the north (~ 95 – 170 km, e.g., Konopliv et al., 2020). At such resolutions, crustal porosity is difficult to decouple from crustal thickness and elastic thickness variations based on gravity and topography inversions alone (Genova et al., 2023; Goossens et al., 2022). Given the similarity in size between the Moon and Mercury and the lack of major erosion processes on both planetary bodies, a lunar-like relationship between Mercury's crater population and crustal porosity can be expected. Here, we use the crater population of Mercury to constrain lateral porosity variations in the planet's cratered terrains applying a parametrization for impact-induced brecciation and subsequent porosity reduction through time (Huang et al., 2022). Regions affected by smooth plains volcanism are treated separately and porosity differences with the cratered terrains are discussed. Our inferred porosity maps are compared to local estimates from gravity and topography, where gravity data are well resolved (Genova et al., 2023), to infer the best fit parameters relating the crater population to the crustal porosity. Crustal thickness models that consider porosity and grain density variations are then constructed, thereby providing valuable insights into the structure of Mercury's crust in the framework of the upcoming BepiColombo mission (Benkhoff et al., 2021).

2. Crustal Porosity From the Impact Population on Mercury's Cratered Terrains

Crustal porosity can be distinguished into two categories, the primary porosity resulting from the crystallisation of the host rock (Tullborg & Larson, 2006) and the secondary porosity, dominantly generated by impact processes blasting and fracturing the crust (Melosh et al., 1992; Wiggins et al., 2022). In porous terrains, porosity is thought to decrease as the surface ages due to various processes including subsequent smaller impacts shaking, melting, and compacting the crust (Milbury et al., 2015; Wünnemann et al., 2008), overburden pressure, and viscous relaxation (Gyalay et al., 2020). This complex interplay was modeled at long-wavelengths for the feldspathic crust of the lunar highlands in a study by Huang et al. (2022). In that work, the surface porosity at latitude and longitude (θ, ϕ) is defined as

$$P(N^{20}, D, \theta, \phi) = \begin{cases} P_0(D)e^{-N_{\theta,\phi}^{20}/C} & \text{if } \bar{d}_{\theta,\phi} \leq D/2 \\ \mathcal{F}(P_{\theta,\phi}^{pre}) & \text{if } D/2 < \bar{d}_{\theta,\phi} < 3.5D/2 \\ P_{init}e^{-N_{\theta,\phi}^{20}/C} & \text{if } \bar{d}_{\theta,\phi} \geq 3.5D/2. \end{cases} \quad (1)$$

In this equation, $P_0(D)$ is the initial basin size-dependent porosity, defined as $D \times S + P_{min}$, where S is a size-dependent porosity parameter and P_{min} is a minimum porosity value, both of which are free parameters. The N^{20} parameter is a laterally variable N (20) count value (i.e., the number of craters with diameter >20 km per 10^6 km²), which is related to the age of the surface (Neukum et al., 2001), and C is a compaction efficiency parameter. The P_{init} parameter defines the model starting porosity and $\bar{d}_{\theta,\phi}$ represents the distance between the point at which porosity is estimated and the closest large basin center ($D > 200$ km). The symbol \mathcal{F} represents a function that converts the pre-impact pre-existing porosity (P^{pre}) to the impact-derived porosity in the vicinity of the basin.

For this model, the porosity generated within a basin is constant and independent of the initial crustal porosity. For regions located within 3.5 radii of any large basin center, the porosity decrease, defined by \mathcal{F} , follows a natural logarithmic taper fitting the impact-generated porosity at the basin rim and the pre-impact porosity at 3.5 radii from the center (Huang et al., 2022).

The above equation is used to model the crustal porosity of Mercury's cratered terrains. Porosity in regions affected by smooth plains volcanism is discussed below. Following Huang et al. (2022), our model starts with an initial global porosity (P_{init}) of 10%. On the Moon, this value was chosen to reflect porosity in the primary crust, resulting from the magma ocean crystallisation (Tullborg & Larson, 2006) and the formation of the South Pole-Aitken basin and other basins early in lunar history (Huang et al., 2022). On Mercury, crater counting statistics indicate that the crust was likely globally resurfaced by volcanism 4.0 to 4.1 billion years ago (Marchi

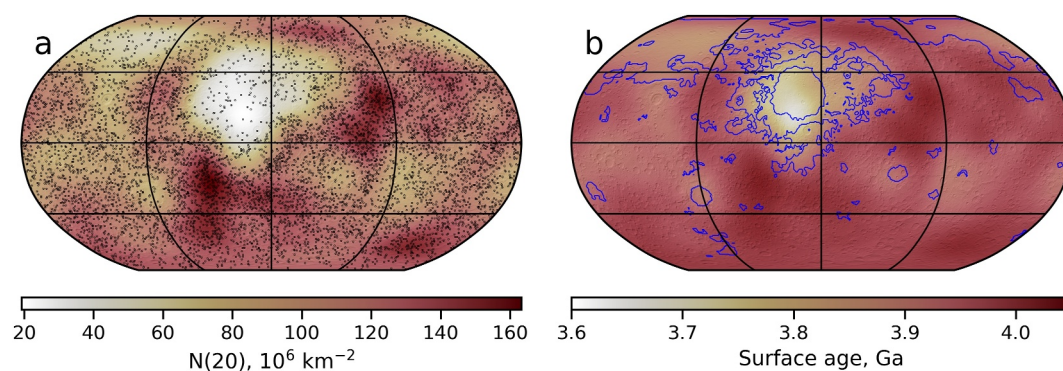


Figure 1. $N(20)$ estimate using a 1,000 km diameter moving window (a) and associated surface age using the Neukum et al. (2001) chronology model (b). Black dots in (a) show the center of craters with diameter >20 km and the blue contours in (b) delimit major smooth plain units (Denevi et al., 2013). The maps are displayed in a Robinson projection centered on 180° longitude and are overlain by a gradient image derived from the topographic model.

et al., 2013). This major event would make most of Mercury's surface akin to an early formed secondary crust. Lacking global porosity constraints on Mercury and details on how this resurfacing event affected the bulk of the crust, we here adopt the same initial porosity as on the Moon. However, we note that this assumption has a minor effect on our porosity maps that are dominated by later impact brecciation (i.e., the secondary porosity). Although uncertainties remain about the formation and evolution of crustal porosity on Mercury, our porosity model will be calibrated using independent gravity-derived porosity maps, as detailed below. This approach enhances our confidence in the model's applicability to the planet.

Similarly to Huang et al. (2022), we only consider that large basins ($D > 200$ km) increase porosity and these are successively formed based either on their estimated age (Orgel et al., 2020), where available, or on our $N(20)$ count. In parallel to this large-basin-inducing porosity phase, the porosity decreases as the surface ages following a parameterized exponential decay (Equation 1). Our $N(20)$ count uses the database of Herrick et al. (2018), which is complete for craters with diameter >5 km. The count is performed using a 1,000 km diameter moving window in order to obtain a smooth $N(20)$ map (Head et al., 2010; Huang et al., 2022). Our $N(20)$ estimates range from 20 to 160 and are consistent with crater counts in large basins from previous work (Figure 1a, Orgel et al., 2020). As expected, low $N(20)$ is found within Mercury's smooth plains, which are thought to be of volcanic origin and younger than the surrounding cratered terrains (Denevi et al., 2013). For reference, our $N(20)$ map is also converted into age using the chronology model of Neukum et al. (2001) and the inferred surface ages of 3.6–4.1 Ga are consistent with earlier work (Figure 1b, Marchi et al., 2013; Orgel et al., 2020).

The study of Huang et al. (2022) highlighted the prominent long-wavelength inverse correlation between the GRAIL-derived porosity and a map of crater density constructed using a 1,000 km diameter counting window. For that reason, our porosity maps are also evaluated on a 1,000 km resolution grid. On the Moon, local scale porosity variations (<200 km wavelength) show more complex patterns with porosity often being lower at the center of medium-sized basins with diameters of 150–300 km (Venkatadri & James, 2020; Wahl et al., 2020). The model described above cannot capture these short-wavelength variations, and we note that these may further be confined to the uppermost crust that was affected by the impact-generated melt pond.

3. Crustal Porosity of Mercury's Smooth Plains

After a planet's early crust forms, subsequent volcanism later in time may largely affect and decrease the pre-existing impact-generated crustal porosity, due to locally enhanced heat flow leading to viscous pore closure (Gyalay et al., 2020) and/or intrusive activity. In addition, while constraints on lunar mare thickness and density exist (e.g., Broquet & Andrews-Hanna, 2024; Gong et al., 2016), the porosity of the maria remains difficult to constrain. Nevertheless, crustal porosity in mare-covered regions is typically found to be smaller ($<10\%$) than in the feldspathic crust ($\sim 20\%$, Kiefer et al., 2012; Goossens et al., 2020). Because of these, regions covered by mare and cryptomare were excluded from the porosity model of Huang et al. (2022) on the Moon.

Similar to the lunar maria, most of Mercury's smooth plains are related to distinct and later volcanism (Denevi et al., 2013; Head et al., 2011), which implies that our porosity model may not be applicable to these regions. For that reason, we conservatively exclude smooth plain regions from our analysis, as has been done for volcanically affected regions on the Moon (Huang et al., 2022). Because smooth plains only cover about 27% of Mercury's surface (Denevi et al., 2013), excluding these regions still allow for our model to constrain a substantial fraction of the planet's crustal porosity.

We have also considered two end-member scenarios that estimate crustal porosity in the smooth plains (Text S1 in Supporting Information S1). For both, we assume that the effect volcanism has on crustal porosity strongly depends on how and where magmatic products were brought to the surface. In a first high-porosity model, we consider that smooth plains volcanism was fed by isolated giant dike systems or mantle plumes, similar to flood volcanism on Earth (Ernst, 2014; Head et al., 2011). In that framework, although volcanism is extensive and widespread, intrusive activity only affected the crust in a few isolated regions within the smooth plains, which we assume to be negligible in area and volume compared to the surrounding crust. As an example, Elysium Planitia on Mars is covered by a thousand kilometres flood lava flow that is thought to originate from a narrow fissure system (Broquet & Andrews-Hanna, 2023; Voigt et al., 2023).

In a second low-porosity model, we assume that intrusive activity and magma rise was widespread and decreased the bulk crustal porosity down to 0% in regions covered by smooth plains. While modeling indicates that large pre-existing crustal porosity can be decreased by subsequent impacts, impacts on a non-porous target can only increase porosity (Huang et al., 2022; Milbury et al., 2015). Therefore, this model assumes that only impacts that post-date smooth plains formation (~ 3.7 Ga, Denevi et al., 2013) have created and increased crustal porosity (Text S1 in Supporting Information S1).

4. Mercury's Crustal Porosity

The basin-generating and time-decreasing porosity parameters of Equation 1 have been constrained on the Moon by fitting the independent GRAIL-derived porosity and were found to be $S = 7.5 \times 10^{-3}$, $P_{\min} = 13.75\%$, $C = 800$ (Huang et al., 2022). For reference, we display how each parameter of Equation 1 affects the crustal porosity in Figure S1 in Supporting Information S1. Unlike the Moon, Mercury's global crustal porosity is mostly unknown. For that reason, our first porosity model uses lunar parameters. In a second model, we fit our porosity maps to locally gravity-derived porosity estimates in the northern hemisphere, where the planetary gravity field is well known (Genova et al., 2023). Because these gravity constraints only cover $\sim 8\%$ of Mercury's surface and in regions that may not be representative of the planet's crust, both porosity models are discussed and retained for further analyses.

Our first model that uses the best-fit lunar parameters displays porosities ranging from 9% to 25% with an average and standard deviation of $14\% \pm 3\%$ (Figure 2). The highest porosity is found in the Caloris region and results from the Caloris impact-induced crustal brecciation. Combining this porosity model with the grain density map determined from geochemical mapping of Beuthe et al. (2020), we obtain bulk crustal densities ranging from 2,150 to 2,790 kg m^{-3} with an average and standard deviation of $2,540 \pm 100 \text{ kg m}^{-3}$ (Table 1).

Our second model is constrained to fit the crustal porosity obtained by Genova et al. (2023) in some regions of Mercury's northern hemisphere. In that study, porosity is determined by comparing the bulk crustal density inverted from a localized admittance model and the observed grain density map of Beuthe et al. (2020). Admittance modeling approach is only reliable in regions where both gravity and topography correlate, and such regions are currently sparse and limited to the northern hemisphere (only $\sim 8\%$ of the planet's surface, Goossens et al., 2022; Genova et al., 2023). In these regions, which encompass both smooth plains and cratered terrains, crustal porosity was constrained to range from 9% to 21% with uncertainties of 1%–5%.

We have performed a grid search over a large parameter space considering all possible combinations of S , C , P_{\min} , and P_{init} . For each combination, we evaluate the root-mean-square misfit of our porosity map with respect to the gravity-derived porosity model of Genova et al. (2023). The misfit is weighted by both surface area and the porosity uncertainty in the admittance model. The best-fit porosity model uses $S = 1 \times 10^{-3}$, $C = 1150$, and $P_{\min} = 16\%$, and displays porosities ranging from 9% to 18% with an average and standard deviation of $13\% \pm 2\%$ (Figure 2). For this model, crustal porosity is slightly lower, though consistent with the model using lunar parameters. The root-mean-square difference between this model and the gravity-derived porosity estimates

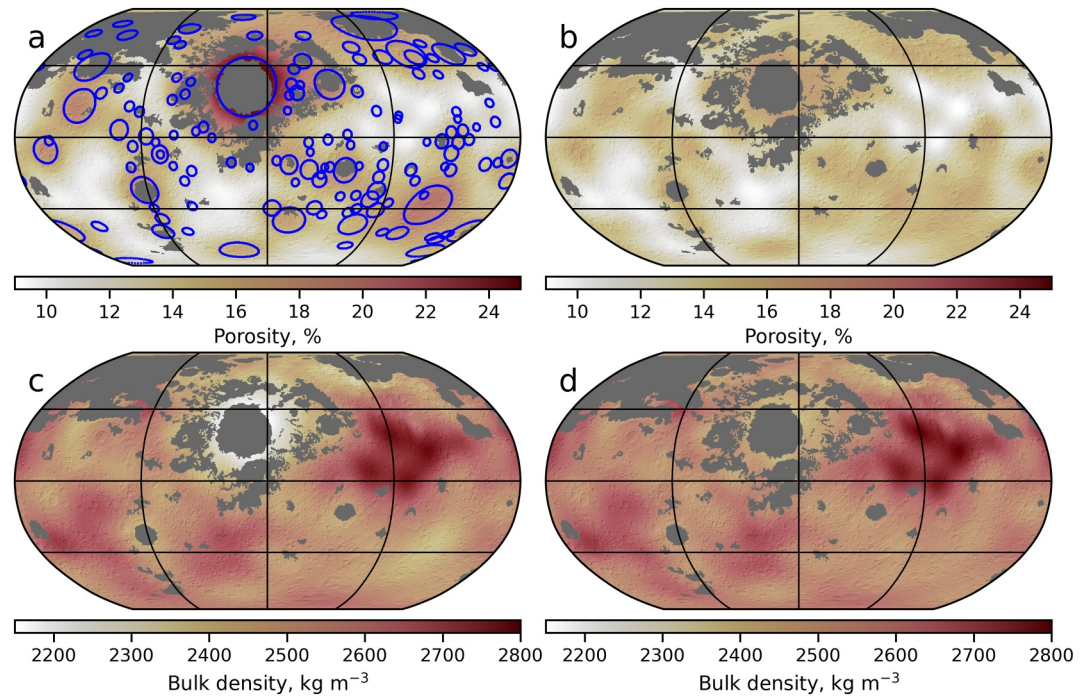


Figure 2. Crustal porosity in cratered terrains as inferred from the crater population for the best-fit lunar parameters (a) and for the model that best fits gravity-derived crustal porosities (b). Associated bulk density of the crust considering the above porosity maps and grain density estimates (c, d, Beuthe et al., 2020). The blue outline in (a) indicates basins with diameter >200 km and regions covered by major smooth plain units are masked out.

is 2.7% (Figure S2 in Supporting Information S1), which is comparable to the porosity uncertainty reported in Genova et al. (2023). The model using the best-fit Moon parameter is also consistent with the gravity-derived porosity estimates within uncertainties but has a somewhat higher misfit (3.2%, Figure S2 in Supporting Information S1). For the best-fit porosity map, the bulk density of the crust only moderately differs from the above model, with an average of $2,565 \pm 70 \text{ kg m}^{-3}$. Other acceptable porosity maps generally show similar porosities with averages of 10%–16% and standard deviations of $\pm 1\%$ –5%.

Our two models accounting for smooth plains volcanism show distinct porosities in regions covered by smooth plains. In the model that only considers volcanic resurfacing, crustal porosity in smooth plain regions resembles that found in the cratered terrains with a mean and standard deviation of $14\% \pm 2\%$ (Figure S3a in Supporting Information S1). The model that assumes volcanism to have reset crustal porosity in the smooth plains shows drastically lower porosities with an average of $7\% \pm 3\%$ and values $< 2\%$ in some areas including the Caloris basin

Table 1
Summary of Our Estimated Crustal Parameters

Crustal model	Porosity range, %	Porosity $\mu \pm 1-\sigma$, %	Bulk density range, kg m^{-3}	Bulk density $\mu \pm 1-\sigma$, kg m^{-3}	Thickness range, km	Thickness $1-\sigma$, km
Constant density	-	-	2,800	2,800	2–70	9
Be20 + 14% porosity	-	14	2,395–2,710	$2,550 \pm 40$	13–58	6
M1	9–18	13 ± 2	2,435–2,690	$2,555 \pm 50$	12–56	5
M2	9–25	14 ± 3	2,220–2,680	$2,530 \pm 80$	12–57	6
Be20 + M1	9–18	13 ± 2	2,355–2,800	$2,565 \pm 70$	12–67	7
Be20 + M2	9–25	14 ± 3	2,150–2,790	$2,540 \pm 100$	12–67	7

Note. Model M1 provides the porosity model that best fits gravity-derived porosity constraints (Genova et al., 2023), and M2 uses the best-fit lunar parameters (Huang et al., 2022). Be20 models make use of grain density constraints (Beuthe et al., 2020). μ denotes the mean and $1-\sigma$ is the standard deviation. The average crustal thickness in all models is fixed to 35 km.

(Figure S3b in Supporting Information S1). These models reveal that crustal porosity in regions affected by smooth plains volcanism remain difficult to constrain and are not discussed further.

5. Effect of Mercury's Crustal Porosity on Crustal Thickness Inversions

Mercury's crustal thickness is inverted from gravity (Konopliv et al., 2020) and topography (Zuber et al., 2012) data using our inferred porosity and bulk crustal density maps. Because depth-variations of porosity remain largely unconstrained and cannot be captured by our model, we consider porosity to be constant with depth in our crustal thickness inversions. We note that some other studies have considered porosity variations with depth, including models assuming near-zero porosity at the crust-mantle interface (Beuthe et al., 2020). On Mercury, porosity may also affect the upper mantle in regions with thin crust and/or cold mantle. However, because impact-generated porosity in the upper mantle may not be preserved throughout geologic history and because mantle density variations are unknown, such models are not considered here.

To account for Mercury's variable gravity field resolution, we have processed both the gravity and topography data by limiting their spectral expansion to a laterally variable maximum resolution (Figure S4 in Supporting Information S1). The spatially variable resolution is obtained from the degree strength map of Konopliv et al. (2020), which is defined as where the gravity signal of the coefficients of that degree equals the gravity uncertainty or noise. This approach improves upon classical gravity and topography inversions that assume a maximum degree globally (e.g., Beuthe et al., 2020), as it allows exploiting the high-resolution gravity field in the northern hemisphere without biasing the inversion in the south.

Crustal thickness inversions are performed using the DSP package (Broquet, 2024). We note that our finite-amplitude relief corrections make use of topography at its full resolution (i.e., not degree-strength down-sampled). A downward continuation filter with an amplitude of 0.5 at degree 90 was applied to the inversion to damp the small-scale oscillations of the crust-mantle interface (Wieczorek et al., 2013). We assume a mean crustal thickness of 35 km, a mantle density of $3,200 \text{ kg m}^{-3}$, and a crustal grain density of $2,950 \text{ kg m}^{-3}$ (Beuthe et al., 2020; Genova et al., 2023). Because porosity in the smooth plains remain uncertain, our models assume a bulk crustal density of $2,600 \text{ kg m}^{-3}$ in these regions following previous work (Genova et al., 2023; Goossens et al., 2022). When combined with the grain density of smooth plains terrains (Beuthe et al., 2020), this chosen bulk density implies a porosity of 8%, which is consistent with that of the lunar maria (Kiefer et al., 2012) and within the bounds obtained by our two scenarios (Text S1 in Supporting Information S1, Figure S3 in Supporting Information S1).

In our models, crustal thickness is found to range from 12 to 67 km and is generally lowest in the northern hemisphere and within Caloris (Figure 3). In particular, we note that the effect of porosity differences on crustal thickness is about ± 10 km, which is comparable to that from grain density variations (Figure 3, Table 1).

6. Discussion and Conclusions

Knowledge of Mercury's crustal porosity is critical to inferring the planet's geologic, tectonic, and geodynamic evolution through time. Crustal porosity prominently controls the capacity of heat to be conducted through the crust (Gyalay et al., 2020), and thus largely influence the planet's thermal evolution. Lateral variations in crustal porosity can further affect how planetary cooling and global contraction are expressed in the tectonic record (Andrews-Hanna & Broquet, 2023). Variations in the bulk density of the crust are also dominated by crustal porosity, and thus this quantity strongly affects inversions of gravity and topography for crustal thickness (Wieczorek et al., 2013).

Assuming that porosity is generated by large impacts and subsequently decreases with time, our study shows that crustal porosity of Mercury's cratered terrains is similar to that of the Moon, with a range of 9%–18% and an average and standard deviation of $13\% \pm 2\%$. This model was constructed to fit independent gravity-derived porosity maps of Mercury's northern hemisphere (Genova et al., 2023). The Caloris region displays the highest impact-generated porosity ($\sim 18\%$), which resembles that found for the largest lunar basins such as Moscoviense or Orientale (Huang et al., 2022; Soderblom et al., 2015). Considering the best-fit parameters obtained on the Moon by Huang et al. (2022), porosity is found to be comparable with an average of $14\% \pm 3\%$. Although Mercury's crustal porosity remains challenging to constrain, our model fits independent gravity-derived porosities

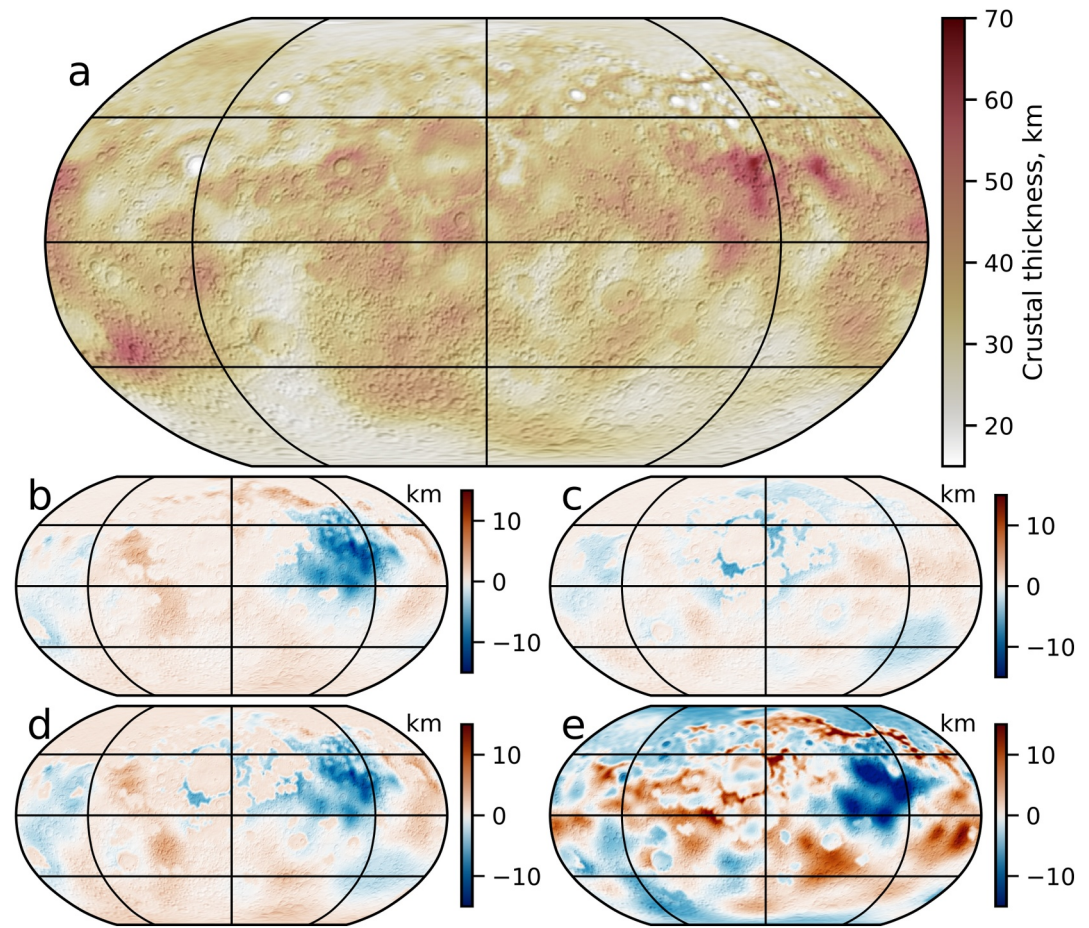


Figure 3. Crustal thickness considering grain density variations and the effect of crustal porosity using the model that best fits gravity-derived porosity constraints (a). Difference between the model in (a) and models considering the same porosity but a constant grain density of $2,950 \text{ kg m}^{-3}$ (b), the best-fit lunar parameters for porosity with lateral grain density variations (c) or constant grain density (d), and considering a constant bulk density of $2,800 \text{ kg m}^{-3}$ (e).

and offers a plausible range of lateral porosity variations, based on a method that has proven successful on the Moon (Huang et al., 2022).

Our modeling approach is not designed to consider porosity variations with depth, although such variability is expected (e.g., Besserer et al., 2014; Beuthe et al., 2020; Gyalay et al., 2020). However, our approach is adequate to infer the depth-integrated bulk porosity of the crust (Huang et al., 2022). Assuming that porosity is zero at the base of the crust (35 km) and decreases with an e -folding depth of 4–12 km (Beuthe et al., 2020; Wiczorek et al., 2013), an average crustal porosity of 13% implies surface porosities of 15%–19%, respectively (Figure S5 in Supporting Information S1).

Accounting for laterally variable crustal porosity and grain density (Beuthe et al., 2020), our models constrain the bulk density of the crust to range from $2,355$ to $2,800 \text{ kg m}^{-3}$, with an average and standard deviation of $2,565 \pm 70 \text{ kg m}^{-3}$. These values are consistent with independent gravity derived bulk densities in Mercury's northern hemisphere (Genova et al., 2023; Goossens et al., 2022) and are similar to that found for the lunar highlands (Goossens et al., 2020; Wiczorek et al., 2013).

We have constructed crustal thickness models accounting for the spatially variable resolution of Mercury's gravity field by adding a pre-processing filter to limit the spectral expansion of the data to the observed gravity field degree-strength (Konopliv et al., 2020). This approach improves upon earlier work that used globally constant resolution (Beuthe et al., 2020; Genova et al., 2019), thereby biasing crustal thickness estimates where the gravity

field is poorly known. Considering porosity and grain density variations, crustal thickness is found to range from 12 to 67 km.

Our crustal thickness models have assumed a mean thickness of 35 km. An alternate approach is to find the minimum average crustal thickness required to have non-negative crustal thicknesses everywhere on the planet (Wieczorek et al., 2022). Under such assumptions, we obtain average crustal thicknesses of ~18 km for all tested models with porosity and/or density variations (Figure S6 in Supporting Information S1).

A year after BepiColombo is inserted into Mercury's orbit, gravity field models are expected to achieve a global resolution of about degree 40 (Iess et al., 2021). At such resolution, additional estimates of the bulk density and porosity of the crust could be derived from admittance models (Genova et al., 2023). Planetary shape models from laser altimetry would also be largely improved (Thomas et al., 2021). Together, these would enable better constraints on global porosity maps, ultimately allowing comparisons of the cratering and porosity-generation processes on the Moon and Mercury.

Data Availability Statement

The porosity, N20, crustal thickness models, and truncated topography are available at Broquet et al. (2024). The DSP package is available at Broquet (2024).

References

- Andrews-Hanna, J., & Broquet, A. (2023). The history of global strain and geodynamics on Mars. *Icarus*, 395, 115476. <https://doi.org/10.1016/j.icarus.2023.115476>
- Benkhoff, J., Murakami, G., Baumjohann, W. e. a., Besse, S., Bunce, E., Casale, M., et al. (2021). BepiColombo - mission overview and science goals. *Space Science Reviews*, 217(90), 90. <https://doi.org/10.1007/s11214-021-00861-4>
- Besserer, J., Nimmo, F., Wieczorek, M. A., Weber, R. C., Kiefer, W. S., McGovern, P. J., et al. (2014). GRAIL gravity constraints on the vertical and lateral density structure of the lunar crust. *Geophysical Research Letters*, 41(16), 5771–5777. <https://doi.org/10.1002/2014GL060240>
- Beuthe, M., Charlier, B., Namur, O., Rivoldini, A., & Van Hoolst, T. (2020). Mercury's crustal thickness correlates with lateral variations in mantle melt production. *Geophysical Research Letters*, 47(9), e2020GL087261. <https://doi.org/10.1029/2020GL087261>
- Broquet, A. (2024). Displacement_strain_planet: Version 0.5.0. <https://doi.org/10.5281/zenodo.4916799>
- Broquet, A., & Andrews-Hanna, J. (2023). Geophysical evidence for an active mantle plume underneath Elysium Planitia on Mars. *Nature Astronomy*, 7, 160169. <https://doi.org/10.1038/s41550-022-01836-3>
- Broquet, A., & Andrews-Hanna, J. (2024). The Moon before mare. *Icarus*, 408, 115846. <https://doi.org/10.1016/j.icarus.2023.115846>
- Broquet, A., Rolser, F., Plesa, A.-C., Breuer, D., & Hussmann, H. (2024). Data for Mercury's crustal porosity as constrained by the planet's bombardment history. <https://doi.org/10.5281/zenodo.13938934>
- Denevi, B. W., Ernst, C. M., Meyer, H. M., Robinson, M. S., Murchie, S. L., Whitten, J. L., et al. (2013). The distribution and origin of smooth plains on Mercury. *Journal of Geophysical Research: Planets*, 118(5), 891–907. <https://doi.org/10.1002/jgre.20075>
- Ernst, R. E. (2014). Introduction, definition, and general characteristics. In *Large igneous provinces* (p. 139). Cambridge University Press.
- Fassett, C. I., Head, J. W., Baker, D. M. H., Zuber, M. T., Smith, D. E., Neumann, G. A., et al. (2012). Large impact basins on Mercury: Global distribution, characteristics, and modification history from MESSENGER orbital data. *Journal of Geophysical Research*, 117(E12). <https://doi.org/10.1029/2012JE004154>
- Genova, A., Goossens, S., Del Vecchio, E., Petricca, F., Beuthe, M., Wieczorek, M., et al. (2023). Regional variations of Mercury's crustal density and porosity from MESSENGER gravity data. *Icarus*, 391, 115332. <https://doi.org/10.1016/j.icarus.2022.115332>
- Genova, A., Goossens, S., Mazarico, E., Lemoine, F. G., Neumann, G. A., Kuang, W., et al. (2019). Geodetic evidence that Mercury has a solid inner core. *Geophysical Research Letters*, 46(7), 3625–3633. <https://doi.org/10.1029/2018GL081135>
- Gong, S., Wieczorek, M. A., Nimmo, F., Kiefer, W. S., Head, J. W., Huang, C., et al. (2016). Thicknesses of mare basalts on the Moon from gravity and topography. *Journal of Geophysical Research: Planets*, 121(5), 854–870. <https://doi.org/10.1002/2016JE005008>
- Goossens, S., Genova, A., James, P., & Mazarico, E. (2022). Estimation of crust and lithospheric properties for Mercury from high-resolution gravity and topography. *Planet. Science Journal*, 3(145), 145. <https://doi.org/10.3847/PSJ/ac703f>
- Goossens, S., Sabaka, T. J., Wieczorek, M. A., Neumann, G. A., Mazarico, E., Lemoine, F. G., et al. (2020). High-resolution gravity field models from GRAIL data and implications for models of the density structure of the moon's crust. *Journal of Geophysical Research: Planets*, 125(2), e2019JE006086. <https://doi.org/10.1029/2019JE006086>
- Gyalay, S., Nimmo, F., Plesa, A.-C., & Wieczorek, M. (2020). Constraints on thermal history of Mars from depth of pore closure below InSight. *Geophysical Research Letters*, 47(16), e2020GL088653. <https://doi.org/10.1029/2020GL088653>
- Head, J. W., Chapman, C. R., Strom, R. G., Fassett, C. I., Denevi, B. W., Blewett, D. T., et al. (2011). Flood volcanism in the northern high latitudes of Mercury revealed by MESSENGER. *Science*, 333(6051), 1853–1856. <https://doi.org/10.1126/science.1211997>
- Head, J. W., Fassett, C. I., Kadish, S. J., Smith, D. E., Zuber, M. T., Neumann, G. A., & Mazarico, E. (2010). Global distribution of large lunar craters: Implications for resurfacing and impactor populations. *Science*, 329(5998), 1504–1507. <https://doi.org/10.1126/science.1195050>
- Herrick, R. R., Bateman, E. M., Crumacker, W. G., & Bates, D. (2018). Observations from a global database of impact craters on Mercury with diameters greater than 5 km. *Journal of Geophysical Research: Planets*, 123(8), 2089–2109. <https://doi.org/10.1029/2017JE005516>
- Huang, Y., Soderblom, J., Minton, D. e. a., Hirabayashi, M., & Melosh, H. J. (2022). Bombardment history of the Moon constrained by crustal porosity. *Nature Geoscience*, 15(7), 531–535. <https://doi.org/10.1038/s41561-022-00969-4>
- Iess, L., Asmar, S., Cappuccio, P. e. a., Cascioli, G., De Marchi, F., di Stefano, I., et al. (2021). Gravity, geodesy and fundamental physics with BepiColombo's MORE investigation. *Space Science Reviews*, 217(21), 21. <https://doi.org/10.1007/s11214-021-00800-3>
- Kiefer, W. S., Macke, R. J., Britt, D. T., Irving, A. J., & Consolmagno, G. J. (2012). The density and porosity of lunar rocks. *Geophysical Research Letters*, 39(7). <https://doi.org/10.1029/2012GL051319>

Acknowledgments

A.B. is funded by the Alexander von Humboldt Foundation. We thank editor Kevin Lewis for handling our paper. We are grateful to Peter James and an anonymous reviewer for their insightful reviews. We thank the BELA Experiment teams at DLR (Institute of Planetary Research) and at University of Bern (Physikalisches Institut, Bern) as well as the BELA Science Team. H.H. acknowledges the support by the BepiColombo project teams at ESTEC, ESOC, and ESAC. Open Access funding enabled and organized by Projekt DEAL.

- Kiefer, W. S., & Murray, B. C. (1987). The formation of Mercury's smooth plains. *Icarus*, 72(3), 477–491. [https://doi.org/10.1016/0019-1035\(87\)90046-7](https://doi.org/10.1016/0019-1035(87)90046-7)
- Knapmeyer-Endrun, B., Panning, M. P., Bissig, F., Joshi, R., Khan, A., Kim, D., et al. (2021). Thickness and structure of the martian crust from InSight seismic data. *Science*, 373(6553), 438–443. <https://doi.org/10.1126/science.abc8966>
- Konopliv, A., Park, R., & Ermakov, A. (2020). The Mercury gravity field, orientation, love number, and ephemeris from the MESSENGER radiometric tracking data. *Icarus*, 335, 113386. <https://doi.org/10.1016/j.icarus.2019.07.020>
- Marchi, S., Chapman, C., Fassett, C. e. a., Head, J. W., Bottke, W. F., & Strom, R. G. (2013). Global resurfacing of Mercury 4.04.1 billion years ago by heavy bombardment and volcanism. *Nature*, 499(7456), 59–61. <https://doi.org/10.1038/nature12280>
- Melosh, H. J., Ryan, E. V., & Asphaug, E. (1992). Dynamic fragmentation in impacts: Hydrocode simulation of laboratory impacts. *Journal of Geophysical Research*, 97(E9), 14735–14759. <https://doi.org/10.1029/92JE01632>
- Milbury, C., Johnson, B. C., Melosh, H. J., Collins, G. S., Blair, D. M., Soderblom, J. M., et al. (2015). Preimpact porosity controls the gravity signature of lunar craters. *Geophysical Research Letters*, 42(22), 9711–9716. <https://doi.org/10.1002/2015GL066198>
- Neukum, G., Oberst, J., Hoffmann, H., Wagner, R., & Ivanov, B. (2001). Geologic evolution and cratering history of Mercury. *Planetary and Space Science*, 49(14), 1507–1521. [https://doi.org/10.1016/S0032-0633\(01\)00089-7](https://doi.org/10.1016/S0032-0633(01)00089-7)
- Orgel, C., Fassett, C. I., Michael, G., Riedel, C., van der Bogert, C. H., & Hiesinger, H. (2020). Re-Examination of the population, stratigraphy, and sequence of mercurian basins: Implications for Mercury's early impact history and comparison with the Moon. *Journal of Geophysical Research: Planets*, 125(8), e2019JE006212. <https://doi.org/10.1029/2019JE006212>
- Smith, D. E., Zuber, M. T., Phillips, R. J., Solomon, S. C., Hauck, S. A., Lemoine, F. G., et al. (2012). Gravity field and internal structure of Mercury from MESSENGER. *Science*, 336(6078), 214–217. <https://doi.org/10.1126/science.1218809>
- Soderblom, J. M., Evans, A. J., Johnson, B. C., Melosh, H. J., Miljkovi, K., Phillips, R. J., et al. (2015). The fractured Moon: Production and saturation of porosity in the lunar highlands from impact cratering. *Geophysical Research Letters*, 42(17), 6939–6944. <https://doi.org/10.1002/2015GL065022>
- Thomas, N., Hussmann, H., Spohn, T., Lara, L. M., Christensen, U., Affolter, M., et al. (2021). The BepiColombo laser altimeter. *Space Science Reviews*, 217(1), 25. <https://doi.org/10.1007/s11214-021-00794-y>
- Tosi, N., Grott, M., Plesa, A.-C., & Breuer, D. (2013). Thermochemical evolution of Mercury's interior. *Journal of Geophysical Research: Planets*, 118(12), 2474–2487. <https://doi.org/10.1002/jgre.20168>
- Tullborg, E.-L., & Larson, S. Å. (2006). Porosity in crystalline rocks A matter of scale. *Engineering Geology*, 84(1), 75–83. <https://doi.org/10.1016/j.enggeo.2005.12.001>
- Venkataadri, T., & James, P. (2020). Variations of porosity in intermediate-sized lunar impact basins. *Icarus*, 352, 113953. <https://doi.org/10.1016/j.icarus.2020.113953>
- Voigt, J. R. C., Hamilton, C. W., Steinbrge, G., Christoffersen, M. S., Nerozzi, S., Kerber, L., et al. (2023). Revealing Elysium planitia's young geologic history: Constraints on lava emplacement, areas, and volumes. *Journal of Geophysical Research: Planets*, 128(12), e2023JE007947. <https://doi.org/10.1029/2023JE007947>
- Wahl, D., Wieczorek, M. A., Wnnemann, K., & Oberst, J. (2020). Crustal porosity of lunar impact basins. *Journal of Geophysical Research: Planets*, 125(4), e2019JE006335. <https://doi.org/10.1029/2019JE006335>
- Watters, T. R., James, P. B., & Selvans, M. M. (2021). Mercury's crustal thickness and contractional strain. *Geophysical Research Letters*, 48(17), e2021GL093528. <https://doi.org/10.1029/2021GL093528>
- Watters, T. R., Robinson, M. S., Bina, C. R., & Spudis, P. D. (2004). Thrust faults and the global contraction of Mercury. *Geophysical Research Letters*, 31(4). <https://doi.org/10.1029/2003GL019171>
- Wieczorek, M. A., Broquet, A., McLennan, S. M., Rivoldini, A., Golombek, M., Antonangeli, D., et al. (2022). InSight constraints on the global character of the martian crust. *Journal of Geophysical Research: Planets*, 127(5), e2022JE007298. <https://doi.org/10.1029/2022JE007298>
- Wieczorek, M. A., Neumann, G. A., Nimmo, F., Kiefer, W. S., Taylor, G. J., Melosh, H. J., et al. (2013). The crust of the Moon as seen by GRAIL. *Science*, 339(6120), 671–675. <https://doi.org/10.1126/science.1231530>
- Wiggins, S., Johnson, B., Collins, G. e. a., Jay Melosh, H., & Marchi, S. (2022). Widespread impact-generated porosity in early planetary crusts. *Nature Communications*, 13(4817), 4817. <https://doi.org/10.1038/s41467-022-32445-3>
- Wünnemann, K., Collins, G., & Osinski, G. (2008). Numerical modelling of impact melt production in porous rocks. *Earth and Planetary Science Letters*, 269(3), 530–539. <https://doi.org/10.1016/j.epsl.2008.03.007>
- Zuber, M. T., Smith, D. E., Phillips, R. J., Solomon, S. C., Neumann, G. A., Hauck, S. A., et al. (2012). Topography of the northern hemisphere of Mercury from MESSENGER laser altimetry. *Science*, 336(6078), 217–220. <https://doi.org/10.1126/science.1218805>